processes

Article

Achieving High Performance with Less Energy Consumption: Intermittent Ultrasonic-Mediated Operation Mode for Fe/V Non-Aqueous Redox Flow Battery

Hui Long [1,2,†], Peizhuo Sun [2,†], Haochen Zhu [2], Qiang Ma [2], Xiaozhong Shen [3], Huaneng Su [2], Cristina Flox [4,*] and Qian Xu [2,3,*]

[1] College of Civil Engineering, Changsha University, Changsha 410022, China; hlong@ccsu.edu.cn
[2] Institute for Energy Research, Jiangsu University, Zhenjiang 212013, China; juaaanzz098@gmail.com (P.S.); 2222393038@stmail.ujs.edu.cn (H.Z.); maqiang@ujs.edu.cn (Q.M.); suhuaneng@ujs.edu.cn (H.S.)
[3] Jiangsu Provincial Engineering Research Center of Key Components for New Energy Vehicle, Wuxi Vocational Institute of Commerce, Wuxi 214153, China; shenxiaozhong@wxic.edu.cn
[4] Department of Electrical Energy Storage, Iberian Centre for Research in Energy Storage, University of Extremadura, Avda. de las Letras, s/n, 10004 Cáceres, Spain
* Correspondence: cristina.flox@ciiae.org (C.F.); xuqian@ujs.edu.cn (Q.X.)
† These authors contributed equally to this work.

Abstract: Deep eutectic solvents (DESs) have attracted much attention as sustainable electrolytes for redox flow batteries. Despite the tremendous advantages of DES-based electrolytes, their high viscosity property has a negative effect on their mass transfer, limiting current density and power density. The ultrasonic effect has been demonstrated as an efficient strategy to improve mass transfer characteristics. Incorporating ultrasonic waves into a deep eutectic solvent (DES) electrolyte enhances the mobility of redox-active ions, thereby accelerating the reaction dynamics of the Fe(III)/Fe(II) redox pair. This enhancement makes it suitable for use in non-aqueous electrolyte-based redox flow batteries. However, it is necessary to consider the loss of ultrasonic on the internal structure of the battery, as well as the loss of battery component materials and ultrasonic energy consumption in practical applications. Moreover, the continuous extension of the duration of ultrasonic action not only hardly leads to a more significant improvement of the battery performance, but is also detrimental to the energy and economic savings. Herein, intermittent ultrasound is used to overcome the quality transfer problem and reduce the operating cost. Good electrochemical performance enhancement is maintained with a roughly 50% reduction in energy consumption values. The mechanism as well as the visualization of the pulsed ultrasonic field on each half cell has been envisaged through fundamental characterization. Finally, the feasibility of interrupted ultrasonic activation applied to Fe/V RFB using DES electrolytes has been demonstrated, demonstrating similar behavior with continuous ultrasonic operation. Therefore, the interrupted ultrasonic field has been found to be a more effective operation mode in terms of energy cost, avoiding alternative undesirable effects like overheating or corrosion of materials.

Keywords: redox flow batteries; deep eutectic solvent; electrochemical performance; sonocatalysis; interrupted operation mode

Citation: Long, H.; Sun, P.; Zhu, H.; Ma, Q.; Shen, X.; Su, H.; Flox, C.; Xu, Q. Achieving High Performance with Less Energy Consumption: Intermittent Ultrasonic-Mediated Operation Mode for Fe/V Non-Aqueous Redox Flow Battery. *Processes* **2024**, *12*, 2576. https://doi.org/10.3390/pr12112576

Academic Editor: Tanja Vidakovic-Koch

Received: 27 September 2024
Revised: 13 November 2024
Accepted: 14 November 2024
Published: 17 November 2024

1. Introduction

The increasing demand for clean and renewable energy at the global level has stimulated the deployment of a wide number of technologies for low-cost and efficient energy storage systems [1]. Among them, redox flow batteries (RFBs) are the most promising and appealing solution within the research and industrial communities due to their unique features [2,3]. The main advantage of RFBs is the decoupled energy and power values, gaining attention in comparison with lithium-ion technology. Additionally, store/release

energy processes are effectively conducted in RFBs by a simple and fast electron transfer process as a redox reaction without involving any physical changes. These unique features make RFBs the most suitable solution to solve the intermittency problem of renewable energy [4,5]. In this fashion, many technologies have been demonstrated and commercialized using vanadium, iron or organic molecules as electroactive species dissolved in aqueous solvents [6]. In recent years, many discoveries have been made about aqueous flow batteries, such as Ni-Zn batteries [7]. However, aqueous RFBs are impeded by the narrow operational electrochemical window (i.e., 1.23 V under standard conditions) to avoid the water splitting and the concomitant low-energy-density values [8]. By contrast, non-aqueous RFBs (NARFBs) have emerged as an alternative approach to achieve greater energy density by widening the operational electrochemical window (up to 2.2 V). Furthermore, the higher operational voltage range provides additional advantages in the design of the stack since lower cells are needed to achieve the voltage output value, making the reactor more compact and reducing the cost of the battery. Among the electrolytes used for NARFBs, organic solvents or ionic liquid are mainly used. However, the organic solvents suffer from high toxicity as the ionic liquids provide limited stability [9,10].

In this big picture, deep eutectic solvents (DESs) are the preferable alternative for their excellent features, such as easy preparation from inexpensive compounds, ecofriendly, non-flammable and biodegradable. This new type of green solvent may provide a real and promising alternative for the deployment of RFBs facing problems related to sustainability and the high price of the traditional aqueous RFBs. Such an outstanding solvent exhibits high viscosity with unsatisfactory ionic conductivity, which is critical for battery applications [11,12]. To overcome this problem, the current state of the art shows several strategies, such as new formulations of electrolytes containing additives. In 2018, Cao et al. investigated the effect of additives on the performance of vanadium redox flow battery electrolytes [13]. Zeng et al. found that the addition of SO_2 as an additive can effectively decrease the viscosity of the ionic liquid [14]. Particularly, a higher content of SO_2 in the electrolyte provokes a sharp reduction in viscosity values.

Furthermore, Xu et al. studied the temperature effect on the performance of DES-based Fe/V RFBs, leading to the conclusion that higher temperatures have a positive effect on the overpotentials of both positive and negative reactions [15,16]. More importantly, as the temperature increases from 25 °C to 55 °C, the viscosity values of both electrolytes dramatically decrease, leading to a significant reduction in the pumping consumption from 138 mW to 22 mW, respectively. Alternatively, sophisticated strategies have been demonstrated using magnetic or ultrasound fields [17]. For instance, Cheng et al. demonstrated that the viscosity of the DES electrolyte can be decreased under the effect of the magnetic field [18]. Particularly, the peak current density associated with the anodic and cathodic processes can be increased by 41.56% and 30.74%, respectively, as the intensity of the magnetic field increases. Another important strategy to improve the viscosity values and mass transfer processes is the application of an ultrasonic field [19].

In fact, the current state of the art contains many examples for the demonstration of the benefits of the electrochemical reaction in terms of mass transport under the ultrasonic action (so-called sonoelectrochemistry). Ultrasonic waves exert a significant influence on the forces that hold molecules together within an electrolyte. The phenomenon of cavitation, which is induced by ultrasound, can weaken the inter-particle forces, leading to the disintegration of particle clusters. Furthermore, ultrasonic energy can disrupt hydrogen bonding within aqueous solutions. As these binding forces are broken, the aggregated particles are released from each other, resulting in a uniform distribution of ultrafine particles throughout the dispersing medium.

However, the application of ultrasonic to the RFBs above had been barely explored. In this regard, previous investigations in our group showed the synergy effect between the application of magnetic and ultrasonic fields to the DES-based Fe/V RFBs [20]. Indeed, an increase of 37.1% in the performance of RFBs was achieved using the combination of both physical fields, while an increase of 8.6% and 20.8% in the performance was obtained

when the magnetic or the ultrasonic field was applied alone, respectively. Because of the high influence of the ultrasonic field on the enhanced performance, we explored its effect as a unique activator of the mass transfer process on RFBs [21]. Herein, the positive effect of the field applied followed a downward trend for the viscosity values and the opposite for the ionic conductivity. The variation in these features affects the ohmic resistance as well as the electron transfer processes, facilitating the redox reaction. To exemplify this effect, the anodic and cathodic peak current densities increase by 19.02% and 18.57%, respectively, when the power applied for the ultrasonic field is used at 0.11 $W \cdot cm^{-2}$ for the Fe-based electrolyte at 25 °C in the DES. The same trend can be observed with the electrolyte resistance and the electron transfer resistance values. Both values experience a sudden descent for the application of ultrasonic action. Particularly, the electrolyte resistance decreases from 96.75 ohm to 58.28 ohm when the power of the ultrasonic field increases from 0 to 0.28 $W \cdot cm^{-2}$. More importantly, the electron transfer resistance drops from 51.21 ohm to 29.19 ohm in the absence and presence of an ultrasonic field (0.28 $W \cdot cm^{-2}$) at 25 °C, respectively. This work takes advantage of these positive results, exploring the feasibility of the sonoactivation implementation in DES-based RFBs to face the high viscosity and mass transfer issues. Certainly, this strategy has been applied in other fields, achieving excellent results [22–26].

Another important factor is that the ultrasonic is an energy consuming process. To overcome this issue, an interrupted mode strategy is used to take advantage of the benefits from sonoelectrochemistry, allowing the process to become more energy-efficient. Particularly, the correlation of the electrochemistry activity of the Fe and V redox couples and the duration of the ultrasonic pulse is investigated, providing enhanced performance in the Fe/V RFBs using the DES.

The electrode reaction equations and potentials of the Fe/V RFB are shown below.

$$\begin{aligned} Fe^{3+} + e^- &\leftrightarrow Fe^{2+} & E^0_{Fe,298K} &= 0.769V \\ V^{3+} + e^- &\leftrightarrow V^{2+} & E^0_{V,298K} &= -0.260V \\ Fe^{2+} + V^{3+} &\leftrightarrow V^{2+} + Fe^{3+} & E^0_{298K} &= 1.029V \end{aligned}$$

2. Experimental

2.1. Preparation of Electrolyte

The deep eutectic solvent (DES) was prepared from choline chloride and ethylene glycol by adjusting the 1:2 molar ratio. The mixture was heated at 40 °C with continuous stirring until a homogenous colorless liquid was formed. Once room temperature was reached, the electrolytes were prepared by a complete solution of the redox-active materials (0.1 M anhydrous VCl_3 or 0.1 M $FeCl_3$) in the DES solvent and used for fundamental electrochemical characterization or RFB testing. (The VCl_3 and $FeCl_3$ were bought from Beijing Vokai® Co., Ltd., Beijing, China).

2.2. Fundamental Electrochemical Measurement

Cyclic voltammetry techniques were used as a fundamental testing technique for the visualization and understanding of the interrupted ultrasonic effect. For that purpose, a thermostated three-electrode cell immersed in an ultrasonic bath was used. A 0.196 cm^2 geometric area of a glassy carbon electrode and a platinum electrode was used as the working electrode and the counter electrode, respectively, while a saturated calomel electrode was used as the reference electrode. The glassy carbon was polished before each experimental measurement using 0.2 mm aluminum powder and then rinsed with deionized water. Herein, the pulse duration of the ultrasonic effect is optimized by applying two sequential ultrasonic on (pulse time) and off (resting time) cycles and measuring the current intensity response as a function of the potential applied. Each cycle is composed of the following steps:

(1) Pulse time, T_p: defined by the duration time for the application of the ultrasonic waves.
(2) Resting time, T_r: defined as the interval of time in the absence of the ultrasonic effect.

After each T_p or T_r, the cyclic voltammetry was collected at several temperatures between the potential range from −0.5 to 1.4 V for the vanadium-based DES electrolyte and from −0.35 to 0.85 V for the Fe-based DES electrolyte at 50 mV/s of scan rate. In all experiments, the temperature was controlled and monitored with a digital thermometer.

2.3. Redox Flow Battery Set Up

The real application of the ultrasonic in a flow battery was studied using a filter-press reactor connected with two reservoirs to store the anolyte and catholyte electrolytes (0.1 M concentration of redox active species was used in a volume of 50 mL of the DES- based electrolyte). Both electrolytes were continuously flowing through the filter-press reactor at 20 mL/min as a flow rate in order to produce the electrochemical reaction. Figure 1 shows a schematic representation of the filter-press cell containing the graphite plates with hydraulic fields as the current collector and graphite felt electrodes (GFA series, SGL®, Nuremberg, Germany) separated by a Nafion 212 membrane (DuPont®, Wilmington, DE, USA). The geometrical area of the electrode membrane sandwich was 1 cm^2. The membrane was previously washed in warm water and later pretreated in 5 wt.% H_2O_2 aqueous solution, warm water and 0.5 M H_2SO_4. Subsequently, the membrane was soaked in the electrolyte overnight. The RFBs were immersed in a temperature-controlled ultrasonic bath, and the two electrolytes were temperature-controlled.

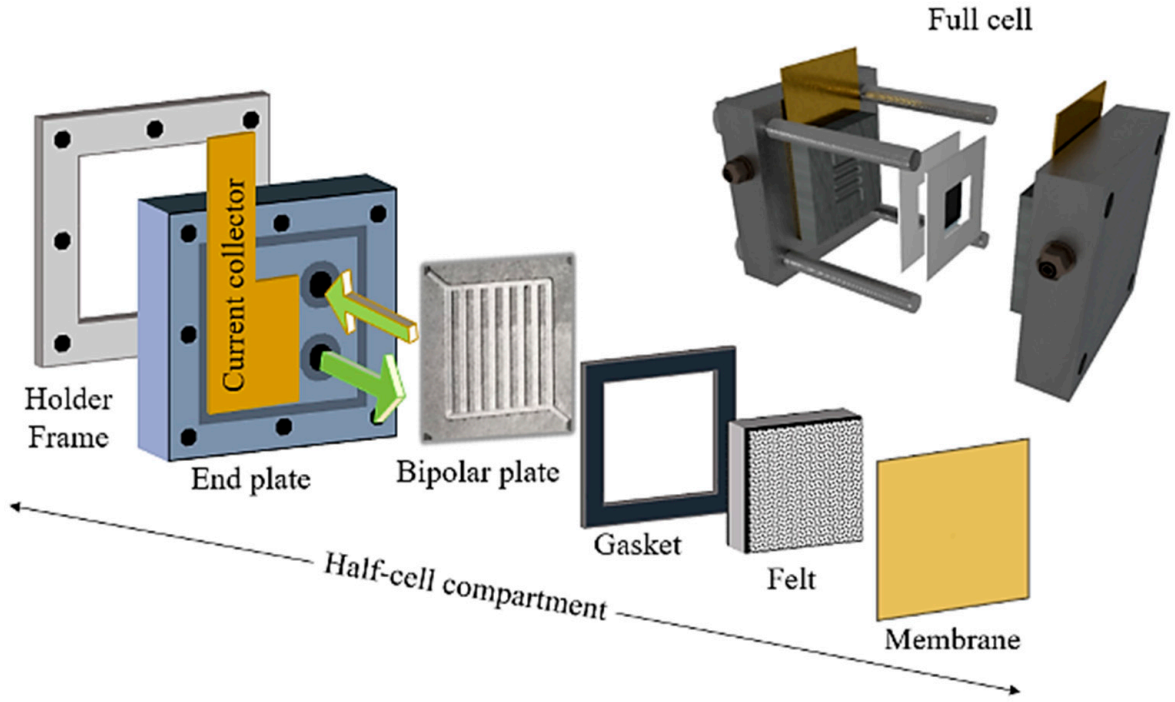

Figure 1. Schematic view of redox flow battery.

Preprocess the graphite felt. Before the experiment, several square graphite felts with sizes of 1 cm × 1 cm are cut and soaked in the DES for a period of time.

The actual experimental setup is shown in Figure 2.

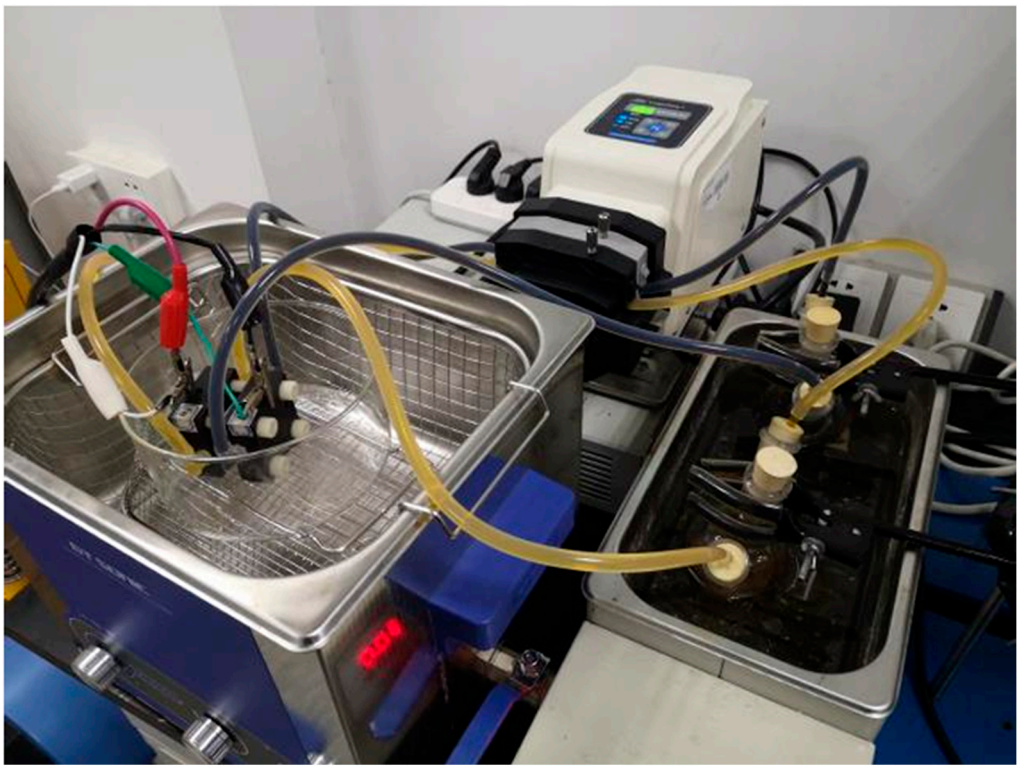

Figure 2. Diagram of ultrasonic action on Fe/V RFB.

3. Results and Discussion

3.1. Individual Study of the Effect of Interrupted Ultrasonic Activation on the Electrolytes

The application of an ultrasonic physical field significantly improves the electrochemical properties of the Fe(III)/Fe(II) and V(III)/V(II) redox couple (as shown in Figure 3). Considering the cost and the problem of electrolyte overheating, we studied the effect of the intermittent ultrasonic application strategy on the performance of a Fe/V flow redox battery. To closely observe the influence of the ultrasonic-mediated activation and visualize the acoustic interrupted cavitation effect over the solid (electrode)/liquid (electrolyte) interface, we conducted a fundamental study on the individual compartments. To this aim, we examined the cyclic voltammetry (CV) after employing two ultrasonic pulses (T_{p1} or T_{p2}: ultrasonic ON) and a resting period (T_r: ultrasonic OFF) between both pulses. Electrochemical parameters have been collected from the CVs as key criteria for evaluating the electrochemical effect of the ultrasonic-mediated process [21]. Particularly, the peak current density (I_p) and peak potential values (E_p) for both processes, oxidation (*a*, anodic) and reduction (*c*, cathodic), as well as the related anodic/cathodic peak currents (I_{pa}/I_{pc}) and peak-to-peak separation (ΔE_p) have been used as key indicators of the performance.

The redox potentials and peak separation values for both the Fe and V systems are shown below (Table 1).

Table 1. The redox potentials and peak separation values for both the Fe and V systems.

Potential vs. SCE in DES (V).	Reduction Potential	Oxidation Potential	Peak Separation Values
Fe^{2+} and Fe^{3+} ions	0.170	0.383	0.213 1.937
V^{2+} and V^{3+} ions	−0.610	−0.355	0.255 3.353

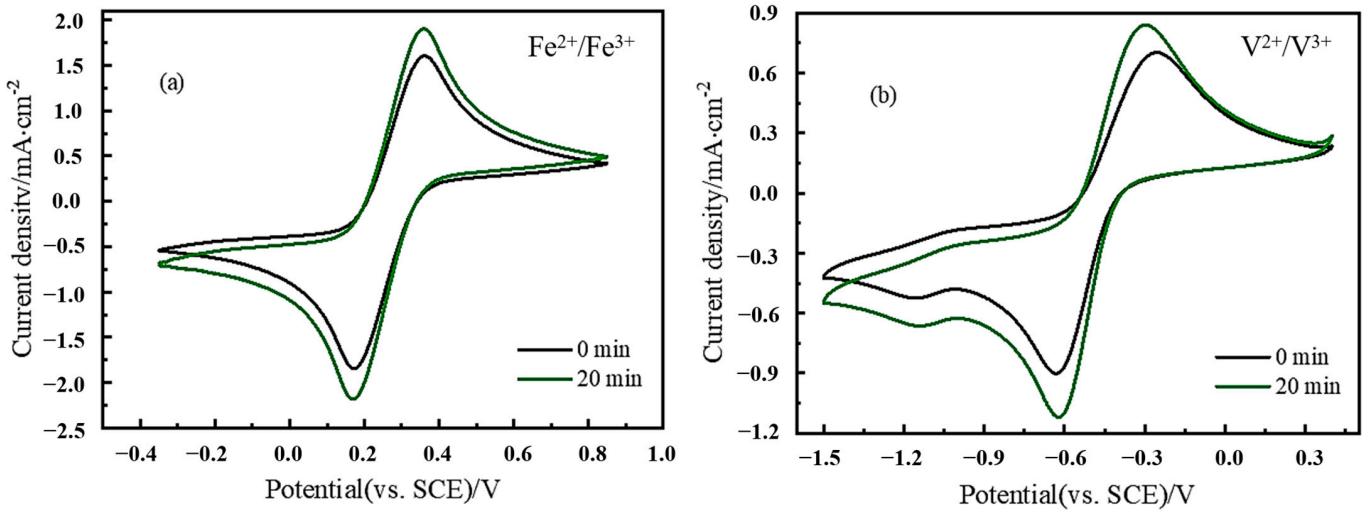

Figure 3. Cyclic voltammetry curves of 0.1 M $FeCl_3$ (**a**) and 0.1 M VCl_3 (**b**). The cyclic voltammetry was collected between the potential range from −0.35 to 0.85 V for the Fe-based DES electrolyte and from −0.5 to 1.4 V for the vanadium-based DES electrolyte at 50 mV/s of scan rate.

Figure 4 illustrates the evolution of the peak current density in the oxidation (I_{pa}) and reduction (I_{pc}) processes for the redox reaction of each compartment (Fe and V as redox species) in the ultrasonic pulses (T_{p1} and T_{p2}) and resting period (T_r). In addition, the electrolyte temperature dependence was evaluated to mitigate the thermal effect of the so-called "hot spots" (i.e., severe temperatures caused by the concentrated energy within the bubble collapse process).

The first observation extracted from the comparison of both half-cells in Figure 4 is a similar general trend in the I_{pa} and I_{pc} along the interrupted ultrasonic application process. Both redox processes exhibit significantly better performance when the time duration T_{p1} increases (presence of ultrasonic waves) as shown by the increase in the peak current density (I_{pa} and I_{pc}) up to a steady state. Note that this effect has been demonstrated in previous works in our laboratories, showing that the ultrasonic activation can effectively improve the Fe(III)/Fe(II) and V(III)/V(II) redox couple.

After stabilization and removing the ultrasonic field (T_r: ultrasonic OFF), the electrochemical performance drops as T_r increases until the initial performance is totally recovered (i.e., T_{p1} for time = 0). Surprisingly, the following pulse applied (T_{p2}) requires a significantly shorter time to achieve the steady state in comparison with the first pulse (T_{p1}), leading to a similar current density enhancement. Particularly, the behavior at 25 °C (orange curve in Figure 4) shows that the steady state peak current density values achieved for T_{p1} in the Fe and V half-cells attain values up to 2.25 (I_{pa})/−2.35 mA·cm^{-2} (I_{pc}) and 0.98 (I_{pa})/−1.16 (I_{pc}) mA·cm^{-2}, respectively. Those values are also quite similar for the T_{p2}: 2.31 (I_{pa})/−2.39 (I_{pc}) mA·cm^{-2} for the Fe half-cell and 0.94 (I_{pa})/−1.13 (I_{pc}) for the V half-cell. Notably, T_{p1} differs widely in comparison with T_{p2} for both half-cells. For instance, T_{p1} for the Fe half-cell requires 9 min for stabilization, being considerably higher than the 5 min for the second pulse (T_{p2}). Similarly, the V half-cell demands 12 min for T_{p1} and 9 min for T_{p2}. Remarkably, the time for recovering the original performance between both pulses (T_r) is 9 min for Fe and 12 min for the V half-cell, suggesting that the ultrasonic effect persists up to that time. These observations agree well with our initial strategy, as the application of interrupted ultrasonic-mediated activation has been experimentally shown to be efficient with concomitant energy savings compared to continuous ultrasonic processes.

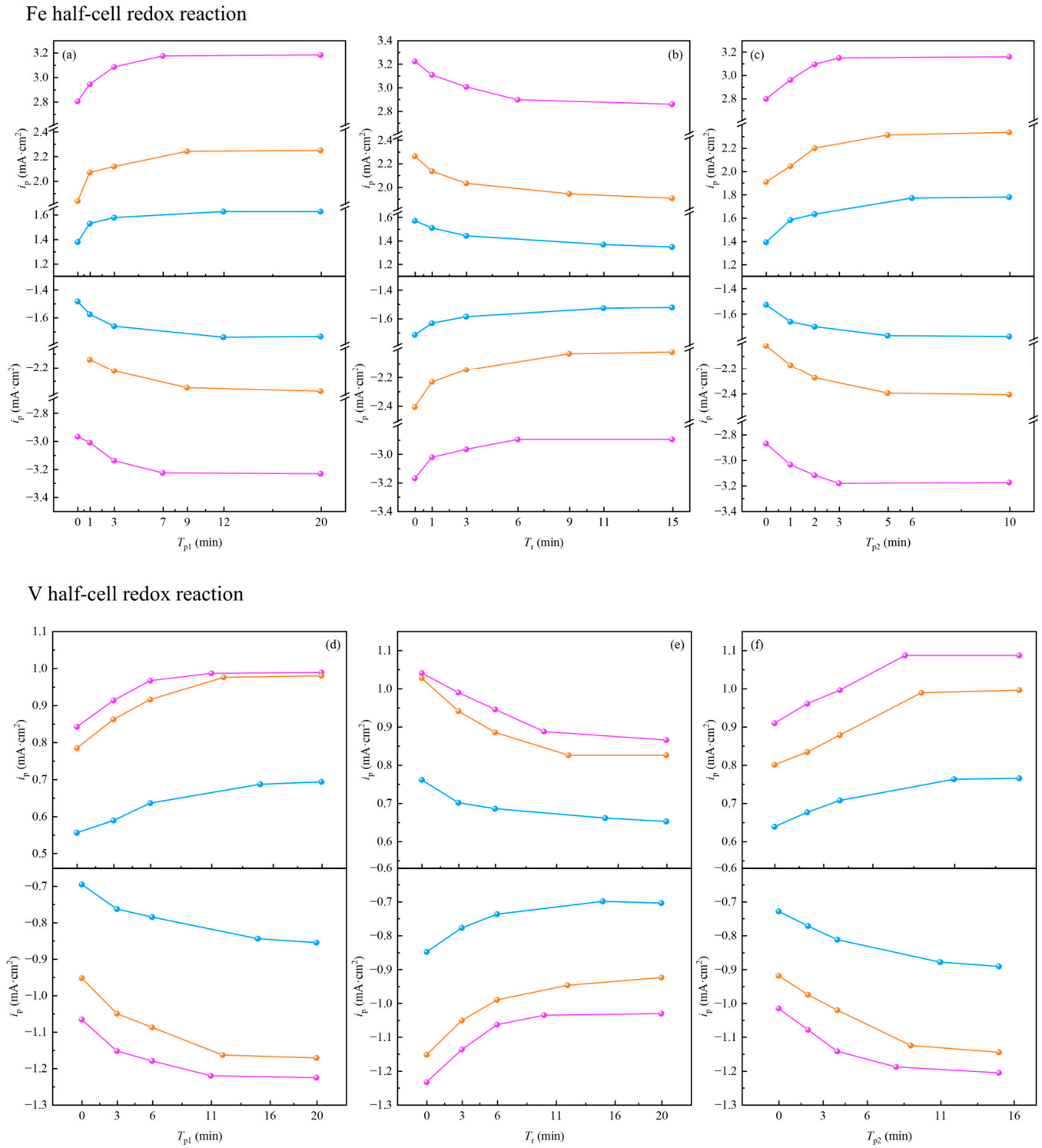

Figure 4. Electrochemical catalytic activity of the Fe (Figure (**a**–**c**)) and V (Figure (**d**–**f**)) half-cells reactions under ultrasonic ON and OFF after T_{p1}, T_r and T_{p2} at different temperatures (15 °C (blue); 25 °C (orange) and 35 °C (purple)): in each half-cell, the upper representation is the oxidation peak current density of the oxidation process and lower representation is the peak current density in the reduction process obtained from the CVs.

To rationalize the ultrasonic effect operating in interrupted mode, we assume the following scenario:

- In the first pulse, the cavitation process promotes the electrochemical performance in each half-cell reaction until the steady state is reached. Herein, the cavitation stream offers several benefits on strengthening the diffusion process and, in consequence, the reaction kinetics. Additionally, the bubble collapse attacks the electrode surface, decreasing the diffusion layer thickness. All these effects promote the electrochemical reactions up to a maximum, where the steady state is achieved. In that point, we understand that the concentration polarization effect has become important, demonstrating that the continuous ultrasonic operation mode is not efficient. Remarkably, the steady state was achieved faster as the temperature increased as a typical diffusion-controlled process.
- In the following rest period and in the absence of ultrasound, the cavitation effect persists for a certain time, although it decreases progressively to the initial state. The fact that the initial electrochemical activity of the electrode returns after a period of time in the absence of the ultrasonic activation is proof that the diffusion layer structure is regenerated after the cavitation collapse (T_{p1}). Basically, a replenishment of reactants/products from the bulk to the surface electrode is taking place, leading to the formation of a fresh solid–liquid interface. This process occurs for a period of time, where the duration to establish the initial condition is quite dependent on the temperature, indicting a remarkable diffusion-controlled step.
- In the second pulse (T_{p2}), the steady state is achieved in a considerably shorter time compared to the first pulse (T_{p1}) with better electrochemical properties in each compartment, probably due to the fact that the electrode surface has been activated along the ultrasonic pulse through the bubble collapse (adsorption of the reactants or products) [27]. To verify this fact, Figure 5 shows a comparison of the related anodic/cathodic peak currents (I_{pa}/I_{pc}) and peak-to-peak separation (ΔE_p) under the influence of T_{p1} and T_{p2} acquired for CVs from [21]. Largely, the T_{p2} provides a better electrochemical performance since better values of I_{pa}/I_{pc} (i.e., closer to the unity) and lower ΔE_p values in both half-cells can be achieved in the majority of the cases. Even though the steady state is achieved with similar peak current densities values found between T_{p1} and T_{p2}, the electron transfer process presents better properties in T_{p2}.

Another observation is that the mass transfer limitations become more obvious in the V half-cell rather than the Fe half-cell. For the lower steady state current density obtained for the V half-cell in comparison with the Fe half-cell within T_{p1} and T_{p2}, this fact indicates that the ultrasonic-mediated process has a lesser effect in V rather than the Fe half-cell. The difference in T_r for different ions stems from their different mean square displacement and diffusion coefficients in the DES electrolyte [28]. In addition, the temperature dependencies in both reactions are quite different, as shown in Figure 6. Respectively, higher (35 °C) or lower (15 °C) temperatures provoke a shorter or longer variation to reach the steady state along T_{p1}, T_{p2} and T_r. It is well known that higher temperatures improve the diffusion of the redox species to electrodes, while the contrary effect is taking place at the lower temperatures. Comparing both compartments (Figures 4 and 5), the influence of the higher temperatures is more pronounced in the Fe electrolyte than in the V electrolyte. Those differences between each compartment are ascribed to the higher stokes radius of V in comparison with Fe in the DES electrolyte, affecting the diffusion coefficient and mass transport features. Particularly, the diffusion coefficient of Fe in the DES electrolyte has been determined as ca. 10^{-8} $cm^2 \cdot s^{-1}$, which is one order of magnitude lower than that of V (i.e., 10^{-7} $cm^2 \cdot s^{-1}$) [29,30]. These preliminary findings direct our motivation toward the real implementation of ultrasonic interrupted fields in RFBs to address the importance of efficient operation, boosting the performance of Fe-V RFBs with the concomitant reduction of power consumption.

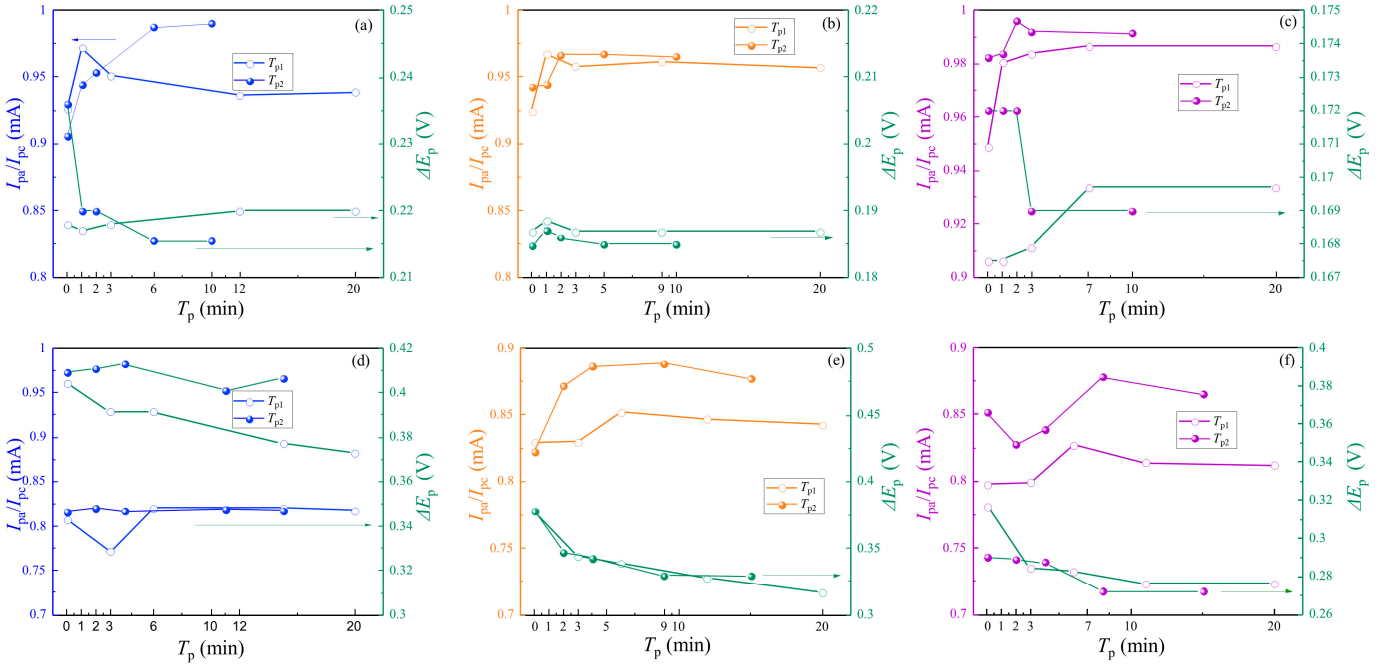

Figure 5. Evolution of key performance indicators upon the first (T_{p1}) and second pulse (T_{p2}) for the Fe half-cell (**a**–**c**) and the V half-cell (**d**–**f**): related anodic/oxidation peak current intensity (I_{pa}/I_{pc}) and peak-to-peak separation (ΔE_p).

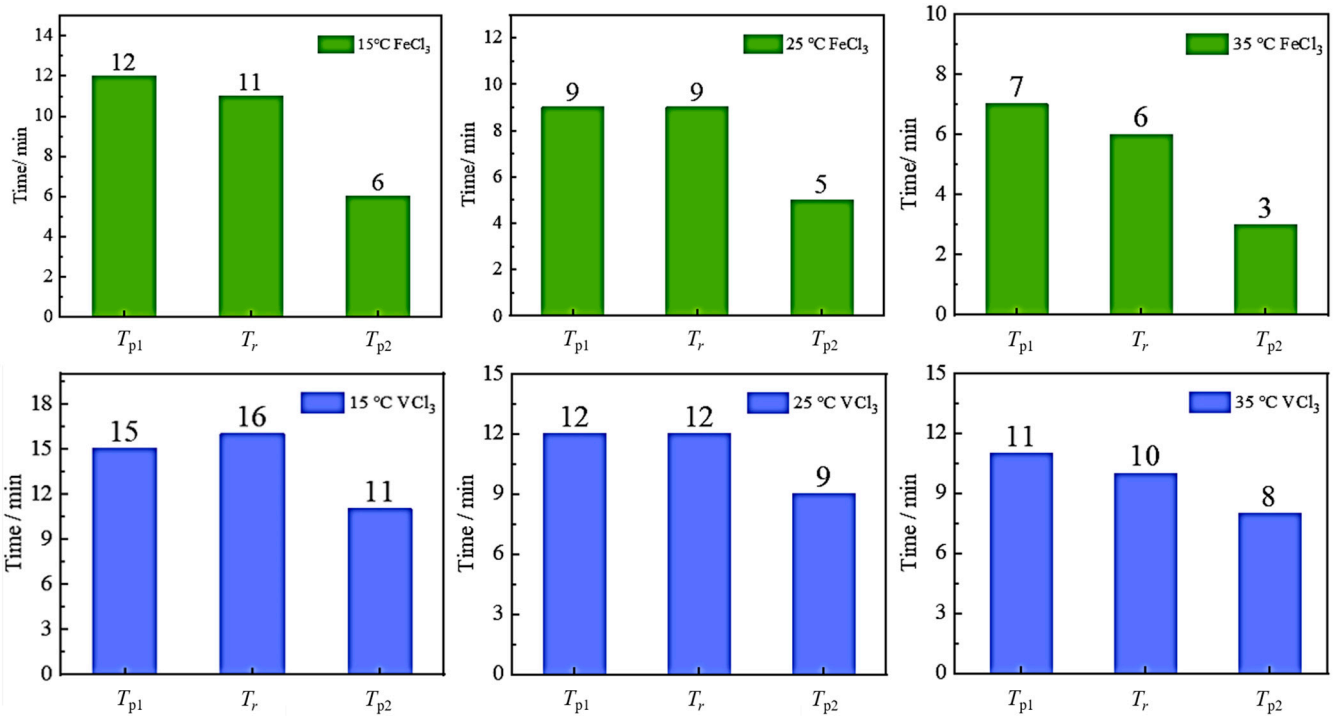

Figure 6. The time required for the active substance to reach a stable state under various modes at different temperatures.

3.2. Practical Operation of Fe/V RFBs Under Continuous and Interrupted Ultrasonic Mode

By selecting the pulse duration, a performance assessment of the Fe/V RFB operating with continuous and interrupted ultrasonic effect has been demonstrated to prove future implementations. Figure 7 shows the voltage profile of the Fe/V RFBs operating in continuous (pink curve) and interrupted (green curve) ultrasonic activation at 2.5 mA·cm^{-2},

corresponding to three cycles (30 min charge and 30 min discharge) and compared with the normal operation (grey curve). From previous studies, 0.11 W·cm^{-2} has been chosen as the ultrasonic power density and 9:9 min as the duty cycle (i.e., 9 min for the ultrasonic ON (pulse time, T_p) and 9 min in OFF (resting time, T_r)). Comparing all curves in Figure 7, the RFB with the ultrasonic-driven process operates at more stable potential values, presenting a flat profile with less polarization (i.e., voltage variations along the 30 min of charge or discharge). Additionally, the ultrasonic effect decreases the overpotentials in both processes up to ca. 40 mV in the charge and 20 mV in the discharge process. This fact is due to the improvement of the mass transfer provided by the ultrasonic effect with the concomitant enhancement of the electrochemical activity. Comparing both curves operating under the ultrasonic effect (i.e., continuous and interrupted mode), the overpotential values are quite similar in all cycles (Figure 7b), albeit, in some points, the interrupted ultrasonic mode exhibits values that are 10 mV higher. This fact is also reflected in the energy efficiency (EE) values (Figure 7c). A significant improvement in the EE resulted from Fe-V RFBs operating with ultrasonic effect. Particularly, the EE increased from 71.9% to 76.2% and 77.4% in the first cycle, operating in normal conditions, interrupted ultrasonic and continuous ultrasonic mode, respectively. More importantly, the EE loss from the first cycle to the second is considerably higher when the RFB operates in the continuous ultrasonic (ca. 1.7%) mode compared to the pulse ultrasonic mode (1.1%). However, ca. 1.5% of the EE was lost in the following cycle under ultrasonic activation, independently of the operation mode.

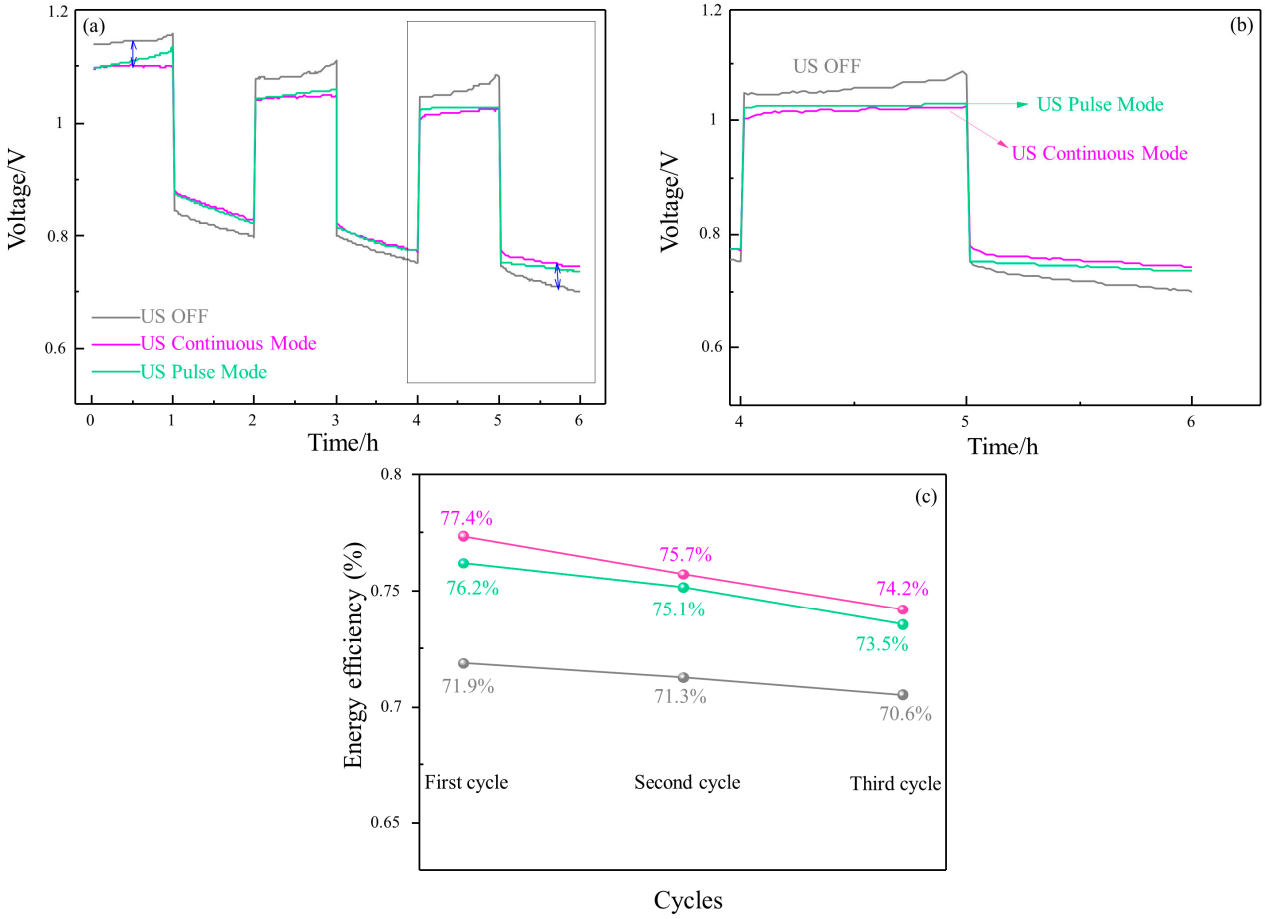

Figure 7. (**a**) Voltage profile of the three 30 min cycles at 2.5 mA·cm^{-2} of the Fe-V RFBs under several operating modes: ultrasonic OFF (grey line); ultrasonic in continuous mode (pink line); ultrasonic in pulse mode (green line); (**b**) Voltage profile of the third cycle showing the overpotentials; and (**c**) energy efficiencies for each cycle in (**a**).

Significantly, the ultrasonic action working in the continued or interrupted mode showed the same performance, making the interrupted mode more beneficial in terms of energy consumption. Particularly, the energy consumption can be reduced up to three times per hour using the 9:9 cycle, making it an economical approach for future applications in RFBs. Additionally, the interrupted mode could be optimal since it prevents the bulk electrolyte from overheating or other undesirable reactions being caused for continuous operations.

4. Conclusions

This study is mainly aimed at the application strategy of ultrasound to carry out related experiments because external ultrasound sees large energy consumption. Therefore, the application strategy was studied to reduce energy consumption while maintaining the original electrochemical performance. Herein, the interrupted operation mode is applied as an efficient strategy to improve the performance of Fe/V redox flow batteries (RFBs). Fundamental studies based on cyclic voltammetry have shown the benefits of the cavitation effect working in interrupted mode, providing reinforcement of the mass transfer process, minimizing the concentration polarization and improving the redox reactions. In the big picture, the performance of individual half-cell reactions in Fe/V RFBs was optimized according to the duration of the ultrasonic pulse, allowing us to understand and visualize the ultrasonic effect in the interrupted mode. In the first pulse, the mass transfer is intensified, promoting the electrochemical reactions up to a steady state. Following a resting period, the ultrasonic effect persists, and the solid/liquid interface is restored. In the second pulse, the new and fresh interface presents better features, allowing for better performance. These findings prove the important role of the duration of the pulse to face high ultrasonic energy consumption.

Clearly, the charge/discharge experiments carried out in both modes (continuous and interrupted ultrasonic field with duty cycle 9:9) present similar behavior in terms of over voltages and energy efficiency. Furthermore, good electro-chemical performance enhancement is maintained with a more than 50% reduction in energy consumption for the interrupted mode, thus favoring the flow battery system efficiency and life span.

This work provides a new insight into ultrasonic application on RFBs, visualizing the ultrasonic effect and mechanism over the solid/liquid interface as a consequence of the interrupted field, thus providing new innovations towards higher performance non-aqueous Fe/V RFBs.

Author Contributions: Conceptualization, H.L. and P.S.; methodology, H.L., P.S. and Q.X.; investigation, H.L., P.S., Q.M. and Q.X.; resources, Q.M., X.S. and H.S.; writing—original draft preparation, H.L.; writing—review and editing, P.S., H.Z. and Q.X.; supervision, X.S., H.S., C.F. and Q.X.; project administration, H.S., C.F. and Q.X.; funding acquisition, H.L., H.S. and Q.X. All authors have read and agreed to the published version of the manuscript.

Funding: Project Funded by Jiangsu Natural Science Foundation (No. BK20231323), Hunan Provincial Natural Science Foundation (No. 2022JJ40525), and National Natural Science Foundation of China (No. 52276066). C.Flox acknowledges financial support from Plan de Recuperación, Transformación y Resiliencia, funded by the European Union NextGenerationEU.

Data Availability Statement: The original contributions presented in the study are included in the article; further inquiries can be directed to the corresponding authors.

Conflicts of Interest: The authors declare that they have no known competing financial interests or personal relationships that could have appeared to influence the work reported in this paper.

References

1. Fagiolari, L.; Sampò, M.; Lamberti, A.; Amici, J.; Francia, C.; Bodoardo, S.; Bella, F. Integrated energy conversion and storage devices: Interfacing solar cells, batteries and supercapacitors. *Energy Storage Mater.* **2022**, *53*, 400–434. [CrossRef]
2. Arenas, L.F.; de León, C.P.; Walsh, F.C. Redox flow batteries for energy storage: Their promise, achievements and challenges. *Curr. Opin. Electrochem.* **2019**, *16*, 117–126. [CrossRef]

3. Zhang, H.; Lu, W.; Li, X. Progress and Perspectives of Flow Battery Technologies. *Electrochem. Energy Rev.* **2019**, *2*, 492–506. [CrossRef]
4. Arévalo-Cid, P.; Dias, P.; Mendes, A.; Azevedo, J. Redox flow batteries: A new frontier on energy storage. *Sustain. Energy Fuels* **2021**, *5*, 5366–5419. [CrossRef]
5. Olabi, A.G.; Allam, M.A.; Abdelkareem, M.A.; Deepa, T.D.; Alami, A.H.; Abbas, Q.; Alkhalidi, A.; Sayed, E.T. Redox Flow Batteries: Recent Development in Main Components, Emerging Technologies, Diagnostic Techniques, Large-Scale Applications, and Challenges and Barriers. *Batteries* **2023**, *9*, 409. [CrossRef]
6. Sun, C.; Negro, E.; Nale, A.; Pagot, G.; Vezzù, K.; Zawodzinski, T.A.; Meda, L.; Gambaro, C.; Di Noto, V. An efficient barrier toward vanadium crossover in redox flow batteries: The bilayer [Nafion/$(WO3)_x$] hybrid inorganic-organic membrane. *Electrochim. Acta* **2021**, *378*, 138133. [CrossRef]
7. Poongodi, A.; Swathi Tharani, D.; Ruby, A.; Manickam, M.; Sivasubramanian, R. Synthesis of Amorphous Nickel-Cobalt Hydroxides for Ni−Zn Batteries. *Chem. Eur. J.* **2024**, e202402325. [CrossRef]
8. Sinclair, N.; Poe, D.; Savinell, R.F.; Maginn, E.J.; Wainright, J.S. A Nitroxide Containing Organic Molecule in a Deep Eutectic Solvent for Flow Battery Applications. *J. Electrochem. Soc.* **2021**, *168*, 020527. [CrossRef]
9. Nayanthara, P.S.; Sreenath, S.; Dave, V.; Kumar, P.; Verma, V.; Nagarale, R.K. Investigation of modified deep eutectic solvent for high performance vanadium redox flow battery. *Electrochim. Acta* **2024**, *508*, 145242. [CrossRef]
10. Chakrabarti, B.; Rubio-Garcia, J.; Kalamaras, E.; Yufit, V.; Tariq, F.; Low, C.T.J.; Kucernak, A.; Brandon, N. Evaluation of a Non-Aqueous Vanadium Redox Flow Battery Using a Deep Eutectic Solvent and Graphene-Modified Carbon Electrodes via Electrophoretic Deposition. *Batteries* **2020**, *6*, 38. [CrossRef]
11. Cao, X.; Wang, S.; Xue, X. A Zn−Ce Redox Flow Battery with Ethaline Deep Eutectic Solvent. *Chemsuschem* **2021**, *14*, 1747–1755. [CrossRef] [PubMed]
12. Zhang, C.; Zhang, L.; Ding, Y.; Guo, X.; Yu, G. Eutectic Electrolytes for High-Energy-Density Redox Flow Batteries. *ACS Energy Lett.* **2018**, *3*, 2875–2883. [CrossRef]
13. Cao, L.; Skyllas-Kazacos, M.; Menictas, C.; Noack, J. A review of electrolyte additives and impurities in vanadium redox flow batteries. *J. Energy Chem.* **2018**, *27*, 1269–1291. [CrossRef]
14. Zeng, S.; Zhang, X.; Gao, H.; He, H.; Zhang, X.; Zhang, S. SO2-Induced Variations in the Viscosity of Ionic Liquids Investigated by in Situ Fourier Transform Infrared Spectroscopy and Simulation Calculations. *Ind. Eng. Chem. Res.* **2015**, *54*, 10854–10862. [CrossRef]
15. Xu, Q.; Qin, L.; Ji, Y.; Leung, P.; Su, H.; Qiao, F.; Yang, W.; Shah, A.; Li, H. A deep eutectic solvent (DES) electrolyte-based vanadium-iron redox flow battery enabling higher specific capacity and improved thermal stability. *Electrochim. Acta* **2019**, *293*, 426–431. [CrossRef]
16. Xu, J.; Ma, Q.; Xing, L.; Li, H.; Leung, P.; Yang, W.; Su, H.; Xu, Q. Modeling the effect of temperature on performance of an iron-vanadium redox flow battery with deep eutectic solvent (DES) electrolyte. *J. Power Sources* **2020**, *449*, 227491. [CrossRef]
17. Zhang, R.; Zhou, H.; Ma, Q.; Li, Z.; Lu, M.; Su, H.; Yang, W.; Xu, Q. Numerical optimization of magnetic field application scheme for deep eutectic solvent (DES) electrolyte flow battery. *J. Power Sources* **2023**, *586*, 233683. [CrossRef]
18. Cheng, R.; Sun, P.; Su, H.; Yang, W.; Leung, P.; Xu, Q. Effect of exerted magnetic field on the performance of non-aqueous iron-vanadium redox flow battery with deep eutectic solvent (DES) electrolyt. *Electrochim. Acta* **2021**, *399*, 139404. [CrossRef]
19. Jiang, F.; Chen, Y.; Ju, S.; Zhu, Q.; Zhang, L.; Peng, J.; Wang, X.; Miller, J.D. Ultrasound-assisted leaching of cobalt and lithium from spent lithium-ion batteries. *Ultrason. Sonochem.* **2018**, *48*, 88–95. [CrossRef]
20. Lu, L.; Zhou, H.; Sun, P.; Shen, X.; Li, Z.; Ma, Q.; Su, H.; Xu, Q. Synergistic effect of ultrasonic and magnetic fields on the performance of non-aqueous iron-vanadium redox flow battery with deep eutectic solvent electrolyte. *J. Energy Storage* **2023**, *63*, 107036. [CrossRef]
21. Sun, P.; Lu, P.; Xu, J.; Ma, Q.; Zhang, W.; Shah, A.A.; Su, H.; Yang, W.; Xu, Q. The influence and control of ultrasonic on the transport and electrochemical properties of redox couple ions in deep eutectic solvent (DES) for redox flow battery application. *Electrochim. Acta* **2021**, *394*, 139140. [CrossRef]
22. Flannigan, D.J.; Hopkins, S.D.; Suslick, K.S. Sonochemistry and sonoluminescence in ionic liquids, molten salts, and concentrated electrolyte solutions. *J. Organomet. Chem.* **2005**, *690*, 3513–3517. [CrossRef]
23. Wang, M.; Han, Y.; Chu, M.; Chen, L.; Liu, M.; Gu, Y. Enhanced electrochemical performances of cerium-doped Li-Rich $Li_{1.2}Ni_{0.13}Co_{0.13}Mn_{0.54}O_2$ cathode materials. *J. Alloys Compd.* **2021**, *861*, 158000. [CrossRef]
24. Theerthagiri, J.; Madhavan, J.; Lee, S.J.; Choi, M.Y.; Ashokkumar, M.; Pollet, B.G. Sonoelectrochemistry for energy and environmental applications. *Ultrason. Sonochem.* **2020**, *63*, 104960. [CrossRef] [PubMed]
25. Breitbach, M.; Bathen, D. Influence of ultrasound on adsorption processes. *Ultrason. Sonochem.* **2001**, *8*, 277–283. [CrossRef]
26. Shende, T.; Andaluri, G.; Suri, R. Power density modulated ultrasonic degradation of perfluoroalkyl substances with and without sparging Argon. *Ultrason. Sonochem.* **2021**, *76*, 105639. [CrossRef]
27. Klima, J. Application of ultrasound in electrochemistry. An overview of mechanisms and design of experimental arrangement. *Ultrasonics* **2011**, *51*, 202–209. [CrossRef]
28. Wang, H.; Ke, H.; Wang, J.; Yan, F.; Cui, X.; Chen, Y. Mechanism of enhanced lithium-ion transport in solid polymer electrolytes assisted by ultrasonic vibration. *J. Appl. Polym. Sci.* **2022**, *139*, 51960. [CrossRef]

29. Hammond, O.S.; Atri, R.S.; Bowron, D.T.; De Campo, L.; Diaz-Moreno, S.; Keenan, L.L.; Doutch, J.; Eslava, S.; Edler, K.J. Structural evolution of iron forming iron oxide in a deep eutectic-solvothermal reaction. *Nanoscale* **2021**, *13*, 1723–1737. [CrossRef]
30. Zhu, L.; Qi, L.; Yao, K. Mass transfer of positive vanadium ions across cell membrane under magnetoelectric composite field. *CIESC J.* **2016**, *67*, 148–158. [CrossRef]